Transient Characteristics of β-Ga_2O_3 Nanomembrane Schottky Barrier Diodes on Various Substrates

Junyu Lai[1], Jung-Hun Seo[1,] *

[1] Department of Materials Design and Innovation, University at Buffalo, The State University of New York, Buffalo, NY USA 14260.

E-mail: junghuns@buffalo.edu

Received xxxxxx
Accepted for publication xxxxxx
Published xxxxxx

Abstract

In this paper, transient delayed rise and fall times for beta gallium oxide (β-Ga_2O_3) nanomembrane (NM) Schottky barrier diodes (SBDs) formed on four different substrates (diamond, Si, sapphire, and polyimide) were measured using a sub-micron second resolution time-resolved electrical measurement system under different temperature conditions. The devices exhibited noticeably less-delayed turn on/turn off transient time when β-Ga_2O_3 NM SBDs were built on a high thermal conductive (high-*k*) substrate. Furthermore, a relationship between the β-Ga_2O_3 NM thicknesses under different temperature conditions and their transient characteristics were systematically investigated and verified it using a multiphysics simulator. Overall, our results revealed the impact of various substrates with different thermal properties and different β-Ga_2O_3 NM thicknesses on the performance of β-Ga_2O_3 NM-based devices. Thus, the high-*k* substrate integration strategy will help design future β-Ga_2O_3-based devices by maximizing heat dissipation from the β-Ga_2O_3 layer.

Keywords: β- Ga_2O_3 nanomembrane diode, heat dissipation, transient characteristic

1. Introduction

Beta gallium oxide (β-Ga_2O_3) has attracted considerable attention as a next-generation wide-bandgap semiconductor for power device applications, high-frequency devices, and solar-blind photodetectors due to its superior material properties [1, 2], such as an ultrawide bandgap value (>4.8 eV), good carrier mobility (>300 $cm^2v^{-1}s^{-1}$), and critical breakdown electric field (≈ 8 MV cm^{-1})[3, 4]. To date, several β-Ga_2O_3 based field-effect transistors, gigahertz range microwave amplifiers, and solar-blind photodetectors have been successfully demonstrated [5-7]. However, one critical native disadvantage of β-Ga_2O_3 is its extremely low thermal conductivity (*k*) (10~ 25 W/m·K) [8, 9], even compared with other popular wide bandgap semiconductors such as silicon carbide (SiC) at 387 W/m·K [10], aluminum nitride (AlN) at 200 W/m·K [11], and gallium nitride (GaN) at 170 W/m·K [12]. Because the abovementioned applications generate a significant amount of Joule heat during operation [13-15], β-Ga_2O_3 with poor thermal properties would become more pronounced in β-Ga_2O_3 based devices. This would cause an even greater increase in temperature and a nonuniform distribution of dissipated power, thus emerging as one of the most serious concerns in the degradation of variability and reliability in β-Ga_2O_3 based applications. [16-18]

Since thermal management is critically important for the efficient operation of β-Ga_2O_3 based devices, several studies have been performed to address the heat dissipation issue in β-Ga_2O_3. For example, Rimmon et al. [19] and Nell et al. [20] reported a method of reducing the self-heating effect by straining the silicon substrate and target material, leading to an increase in carrier mobility and thus balancing the self-heating effect. However, this technology has the following two main challenges: 1) it is difficult to control the defect densities between the Si interface and 2) the target materials that control Si strains in the relaxation level. Another method by Li et al. [21, 22] and Shi et al. [21, 22] proposed a method of mitigating the low thermal conductivity issue, increasing the thermal boundary conductance, and lowering the thermal resistance of β-Ga_2O_3 with the assistance of metallic or dielectric interfacial layers. Recently, another novel route to manage a β-Ga_2O_3 thermal property was to use a sub-micron thin and freestanding format of β-Ga_2O_3, which also called β-Ga_2O_3 nanomembrane (NM). β-Ga_2O_3 NMs can be tailored as a desired sphoare and then transfer-printed onto any new substrates. [23-27] Thus, efficient heat dissipation from β-Ga_2O_3 is expected when β-Ga_2O_3 NMs are transfer-printed on a high-k substrate. For example, Zheng et al. and Cheng et al. used a single-crystal diamond substrate as a heat dissipator to create the β-Ga_2O_3 NM/diamond structure and successfully characterized the thermal conductivity of β-Ga_2O_3 NM and thermal boundary conductance at the β-Ga_2O_3 NM/diamond interface [8, 28, 29]. Cheng et al. and Yixiong et al. also formed the β-Ga_2O_3 NM/SiC structure to realize a similar cooling effect. [30, 31]

These previous studies, however, primarily focused on the relationship between β-Ga_2O_3 and the substrate. In particular, none of the previous studies investigated the impact of the β-Ga_2O_3 NM thickness.

In this paper, we systematically investigated the relationship between the β-Ga_2O_3 NMs thickness and its time-resolved electrical properties on four different thermal conductivity substrates under different temperature conditions. To understand the transient time characteristics of β-Ga_2O_3 based devices, β-Ga_2O_3 NM based Schottky barrier diodes (SBDs) were built on four different substrates via a micro-transfer printing that has a wide thermal conductivity range, from 0.25 W/m·K to 2200 W/m·K, which includes polyimide, sapphire, Si, and diamond substrate, and is characterized as a transport property of β-Ga_2O_3 NM SBDs under different temperature conditions using a sub-micron second resolution time-resolved electrical measurement system. The devices exhibited noticeably less-delayed turn on/off transient time when β-Ga_2O_3 NM SBDs were transfer-printed on a high-k substrate. We also investigated a relationship between the β-Ga_2O_3 NM thicknesses ranging from 300 nm to 1000 nm and their time-resolved electrical properties, which were verified using the Multiphysics simulator. Our results revealed the impact of various substrates with different thermal properties and different β-Ga_2O_3 NM thicknesses on β-Ga_2O_3 NM-based device performance. Thus, these results can help optimize the structure of various future β-Ga_2O_3 based devices by maximizing heat dissipation from the β-Ga_2O_3 layer.

2. Experimental Section

2.1 Device fabrication process

Figure 1(a) shows the schematic illustration of the device fabrication steps. The fabrication process began with a β-Ga_2O_3 bulk substrate grown by molecular beam epitaxy and moderately Sn doped (concentration of 1×10^{18} cm^{-3}) in the [201] direction. The β-Ga_2O_3 NMs were created by clipping several large segments from the bulk substrate at an angle of 77°, followed by an exfoliation using a well-known taping method. β-Ga_2O_3 segments were easily mechanically exfoliated in the [100] direction due to the weak binding energy in this direction. [24-26, 32] In this step, various β-Ga_2O_3 NM thicknesses can be created by adjusting exfoliation times. Once β-Ga_2O_3 NMs were created, we carefully transfer printed them onto undoped Si, sapphire, diamond, and SU-8 coated polyimide substrates using an elastomeric stamp (polydimethylsiloxane, PDMS). Prior to the transfer, all the substrates were cleaned thoroughly by the sonification process in acetone, isopropyl alcohol, and de-ionized (DI) water for 10

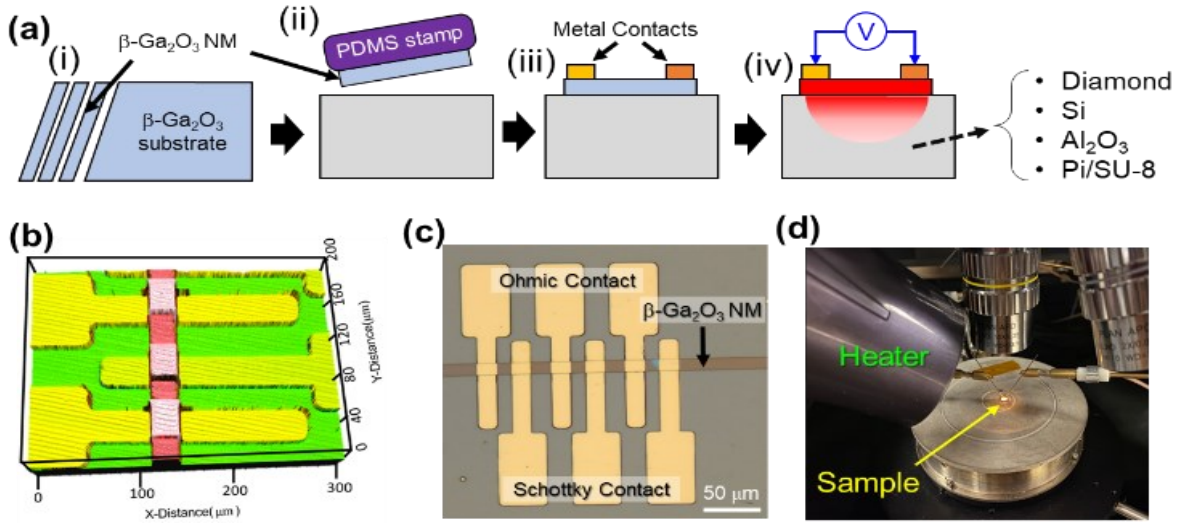

Figure 1. (a) A schematic illustration of the β-Ga_2O_3 NM SBD fabrication process: (i) a creation of β-Ga_2O_3 NMs, (ii) a micro-transfer printing of β-Ga_2O_3 NMs onto four different substrates, (iii) a metallization on β-Ga_2O_3 NMs to form SBDs, (iv) a pulsed I-V characterization. **(b)** Three-dimensional morphology and **(c)** a microscopic image of the fabricated β-Ga_2O_3 NM SBDs **(d)** an image of the heating setup.

min in each step. After the transfer processes were completed, ohmic metal and Schottky metal electrodes deposition processes were conducted. Prior to Ohmic metal deposition, a plasma treatment was performed on β-Ga_2O_3 NMs by a BCl_3/Ar plasma treatment using a reactive ion etcher (RIE) to achieve ohmic contact and to avoid an additional high-temperature annealing process. [25-27] After that, an ohmic metal stack (Ti/Au= 20/100 nm) and a Schottky metal stack (Ti/Pt/Au = 20/30/100 nm) were then deposited to complete the device fabrication.

2.2 Measurement setup

Figure 1(b) and (c) show the three-dimensional (3D) profile and microscopic images of the as-fabricated β-Ga_2O_3 NM SBDs on a diamond substrate to show a generic shape of the β-Ga_2O_3 NM SBDs. Electrical characterization was performed using a Keithley 4200 semiconductor parameter analyzer with a pulsed I-V unit (Keithley 4225-RPM Remote Amplifier/Switch). Voltage–current measurement was conducted at a voltage bias of −3 V to 3 V. To analyze the heat dissipation effect of β-Ga_2O_3 NM SBDs, the pulsed current–voltage (I–V) setup was implemented as follows: the anode bias was pulsed from the off state to the on state. As shown in Figure S2, the pulse width was 500 μs with a pulse period of 1000 μs. The time resolution for a rise and fall time of the pulsed I–V unit was 0.17 μs. All devices were measured using the current compliance setting at 3 mA to prevent unwanted thermal damage. To compare transient time in β-Ga_2O_3 NM SBDs between room temperature (RT) and elevated temperatures, the devices were exposed in heated air and using an incandescent lamp with an objective lens for 10 min to heat the top surface of the device, while the stainless-steel probe station stage remained at 20°C, as shown in Figure (d), and the voltage–current measurement was repeated.

3. Results and discussion

Figure S1 shows I-V curves that were measured from the β-Ga_2O_3 NM SBDs on PI, Si, sapphire, and diamond substrates with different β-Ga_2O_3 NM thicknesses varying from 300 nm to 1000 nm. As shown in Figure S1, all β-Ga_2O_3 NM SBDs exhibited a good rectifying behavior with an on/off ratio higher than ~10^9 times and the ideality factor (n) of , on average, 1.5 ± 0.2, which was calculated based on thermionic emission theory. [33] Similarly good I-V characteristics in β-Ga_2O_3 NM SBDs set a baseline for the time-resolved electrical characterization that relies on different substrates.

Compared with a typical direct current (DC) measurement, an investigation of transient time measurement using a pulsed I-V provides the isothermal condition of the device, thus offering a more accurate power dissipation effect and thermal resistance characteristics. Figure 2 shows the time-resolved pulsed I-V characteristics of the β-Ga_2O_3 NM SBDs on PI, Si, sapphire, and diamond substrates at RT. ~~The devices were biased for 1 mSec with a current compliance of 3 mA to prevent unwanted thermal damage. Details about the measurement setup and an entire pulsed I-V can be found in the Method section and Figure S2 in supplementary document, respectively.~~ The left panel in Figure 2(a)-(c) contains the enlarged plots of transient rise times on different substrates

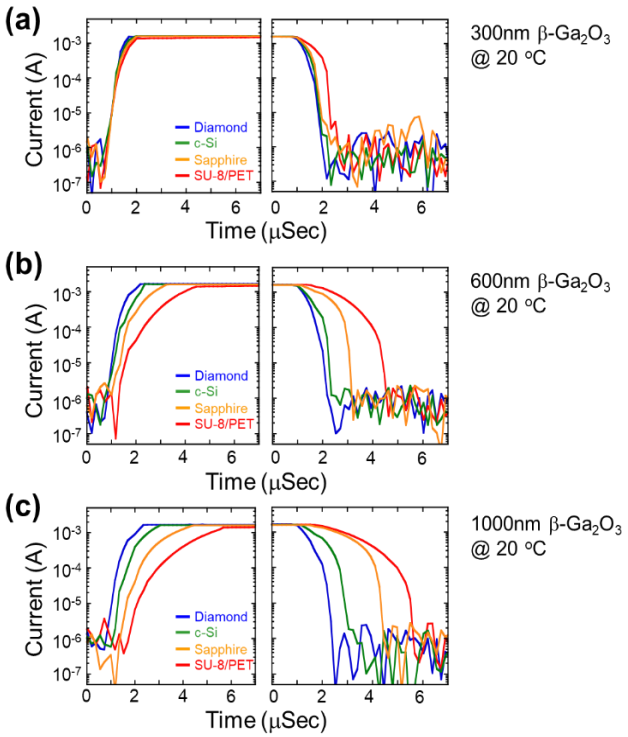

Figure 2. A set of pulsed I-V curves of β-Ga_2O_3 NM SBDs on four different substrates measured at room temperature with three different β-Ga_2O_3 NMs thicknesses **(a)** 300 nm, **(b)** 600 nm, **(c)** 1000 nm, respectively.

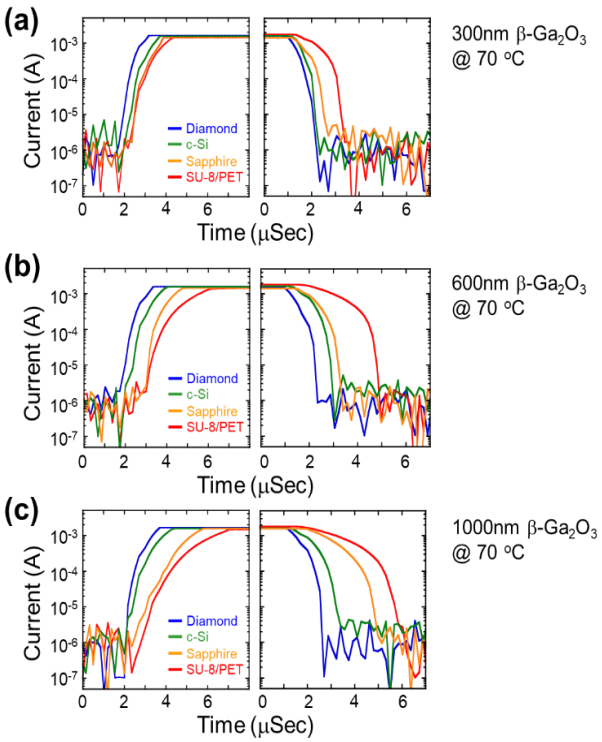

Figure 3. A set of pulsed I-V curves of β-Ga_2O_3 NM SBDs on four different substrates measured at 70 °C with three different β-Ga_2O_3 NMs thicknesses **(a)** 300 nm, **(b)** 600 nm, **(c)** 1000 nm, respectively.

and with different β-Ga_2O_3 NM thicknesses (from 300 nm to 1000 nm). Similarly, the right panel in Figure 2(a)-(c) show the enlarged plots of the transient fall times on different substrates and the same β-Ga_2O_3 NM thicknesses, respectively. The full scale pulsed I-V curves can be found in Figure S2. As shown in Figure 2, the rise and fall time of the devices were noticeably different depending on the substrate. β-Ga_2O_3 NM SBDs on a diamond substrate showed the shortest transient time, followed by the device with Si, sapphire, and PI substrate. The rising time for 300 nm thick β-Ga_2O_3 NM SBDs on the diamond, Si, sapphire, and PI substrates were 1.07 μs, 1.35 μs, 1.4 μs, and 2.65 μs, and their falling times were 1.07 μs, 1.5 μs, 1.65 μs, and 2.85 μs, respectively. Interestingly, the falling time tended to be longer when β-Ga_2O_3 NM SBDs were built on the low-k substrates. The rising and falling time for β-Ga_2O_3 NM SBDs on diamond substrate remained almost the same as 1.07 μs, while the fall time for devices on sapphire and PI substrates were increased compared to their rising from 1.4 μs and 2.65 μs to 1.65 μs and 2.85 μs, respectively. The trapping and de-trapping process in β-Ga_2O_3 NMs and the interaction between β-Ga_2O_3 NM and the substrate can explain this increase in the fall delay characteristic. The trapping and de-trapping process in semiconductors refers to the electron recombining and releasing process for defects or vacancies. Considering that β-Ga_2O_3 has a high level of oxygen vacancies, the trapping and de-trapping process becomes a major source of heat generation in β-Ga_2O_3 NMs. When β-Ga_2O_3 NM SBDs were biased, a Joule heat would be generated from the top surface of β-Ga_2O_3 NMs and begin to accumulate and propagate inside the β-Ga_2O_3 NM which is called a "self-heating" effect. This process supplies sufficient activation energy to overcome the trap potential barrier and escape from the trap, and it is described by equation (1) [34]:

$$J = n\frac{1}{\tau}\exp\left(-\frac{E_i}{kT}\right) \quad (1)$$

Also, the relationship between the trapping time and rising time can be determined by equation (2) [35]:

$$I = 1 - \exp\left(\frac{-t}{\tau}\right)^{\beta} \quad (2)$$

where J is the current density, τ is the trapping / de-trapping time constant, t is the trapping /de-trapping period, E_i is the trap energy, k is the Boltzmann constant, T is the temperature, I is the device on current, and β is the fitting parameter. When combining equations (1) and (2) with the same amount of the on-current, traps with a shorter trapping time constant require shorter times to be filled.

The thermal de-trapping rate is described as follows:[36]

$$k = N_c v \sigma_c \exp\left(\frac{-E_t}{kT}\right)$$

where, N_C is the effective density of states of the material, v is the thermal velocity of carriers, σ_c is the capture cross-section of the trap, E_t is the activation energy, k is Boltzmann's constant, and T is temperature. From this equation, it is shown that the trapped electrons are de-trapped faster when the temperature is the only parameter. However, various parameters also affect the de-trapping rate under elevated temperature. First, the activation energy of β-Ga_2O_3 would be increased as the temperature increases. With higher temperatures, the more defects would be formed, and more dopants would be activated inside the β-Ga_2O_3. The activated Sn dopant atoms in β-Ga_2O_3 are present as Sn^{4+} and preferentially substitute for Ga at the octahedral site. With more gallium vacancies formed and more Sn dopant atoms being activated, the Sn (Sn^{4+}, Sn^{2+}) would not only substitute at the Ga site but also might occupy these Ga vacancies directly and change the charge state and electronic configuration of these defects. This would finally increase the β-Ga_2O_3 activation energy. [37-39] Under biasing conditions, an active region of β-Ga_2O_3 devices becomes heated, and thus trapped electrons are more stable than those at RT [40] because electrons require more energy to overcome the trap barrier. This means that electrons need a longer time to be de-trapped. Second, as reported by Vaidya et al., the time constant to the traps increases with temperature due to the formation of temperature-induced defects. [41]

As a result, the activation energy and temperature-induced defects of β-Ga_2O_3 lead to a longer trapping/de-trapping time constant which in turn causes a time delay in the rise and fall time under heating conditions. Furthermore, such temperature-dependent transient characteristics are severely affected by the thermal conductivity of the substrate—the low thermal conductive substrate inefficiently dissipates heat from the device. Due to the self-heating effect, as temperature increases, the trapping time constant increases and enables these traps to take a longer time to be filled during the charging process. When devices were heated at the same rate and the input power to the device was the same, the rising time for each case did not vary noticeably. However, when the current is stopped, the heat must be dissipated to both air and substrate. The thermal conductivity values of diamond, Si, and sapphire were higher up to 2200, 144, and 40 W/m·K, respectively, compared to that of β-Ga_2O_3 NMs, and the thermal conductivity of PI is substantially lower to 0.25 W/m·K compared to that of β-Ga_2O_3 NMs. [42-45] Thus, their cooling rates are different, therefore, we can conclude that the switching characteristic becomes enhanced when β-Ga_2O_3 NM SBDs are formed on a high-k substrate. This trend is consistent regardless of the thickness of β-Ga_2O_3 NMs (both 300 nm thick and 1000 nm thick β-Ga_2O_3 NMs), as shown in Figure 2.

To further investigate the relationship between delay time, device substrates, and β-Ga_2O_3 NM thickness, the same time-

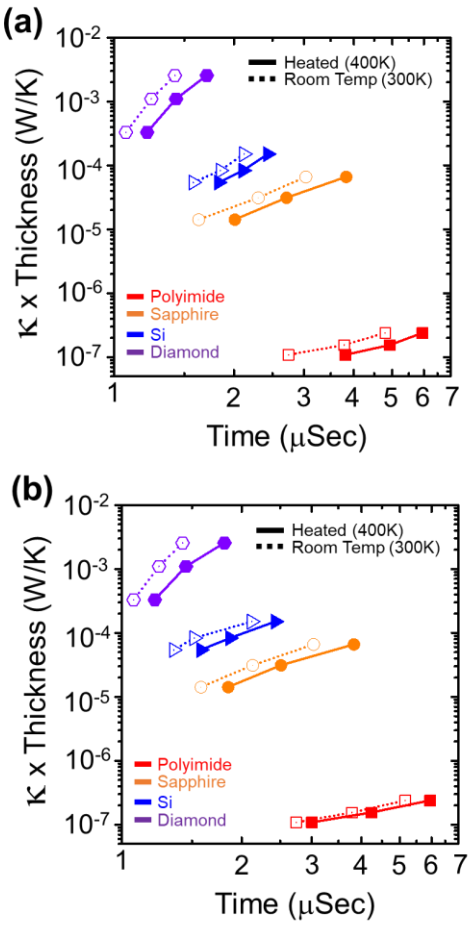

Figure 4. A summary of transient delay times of β-Ga_2O_3 NM SBDs under four different substrates as a function of a product of thermal conductivity of the substrate and thickness of β-Ga_2O_3 NMs, **(a)** a rising delay times, **(b)** a fall delay times.

resolved pulsed I-V characterizations were performed at the elevated temperature. Figure 3 shows the time-resolved pulsed I-V characteristics of the β-Ga_2O_3 NM SBDs on PI, Si, sapphire, and diamond substrates at elevated temperatures. To analyze the heat dissipation effect of β-Ga_2O_3 NM SBDs, devices were heated using the following two heating sources: (1) a focused incandescent light bulb via an objective lens and (2) a heat gun. Both were placed at the top of the device until the top surface reached 70 °C and then the device was biased at 3 V. We repeated this at least three times at RT and 70 °C for transient time characterization. The devices were cooled for a sufficient time (about one-hour intervals). In the left panel of Figure 3(a)-(c), the enlarged plots show the transient rise times on four different substrates and different β-Ga_2O_3 NM thicknesses. Similarly, the right panel of Figure 3(a)-(c) are the enlarged plots of transient fall times on four different substrates and different β-Ga_2O_3 NM thicknesses, respectively. The rising time for 300 nm thick β-Ga_2O_3 NM SBDs on diamond, Si, sapphire, and PI substrates were 1.45

μs, 1.55 μs, 1.65 μs, and 3.4 μs and their falling times were 1.45 μs, 1.6 μs, 1.8 μs, and 3.8 μs, respectively. Similar to the test result at room temperature, the rising and falling time of β-Ga_2O_3 NM SBDs on diamond remained almost the same to be 1.45 μs, while the fall time for devices on the PI substrate increased compared to the rising time from 3.4 μs to 3.8 μs, respectively.

Figure 4(a) and (b) summarize the rising and falling time for β-Ga_2O_3 NM SBDs, respectively, which were extracted from Figures 2 and 3. To provide a clear view of the relationship between the electrical performance of β-Ga_2O_3 NM SBDs with respect to the β-Ga_2O_3 NM thickness and substrate thermal conductivity, a transient delay time was plotted with the product of the β-Ga_2O_3 NM thickness and substrate thermal conductivity (W/K·sec: W/K vs. delay time). Therefore, the slope of the curve indicates the capacity for heat dissipation as well as the rate of the trapping/de-trapping process. For the rising time of β-Ga_2O_3 NM SBDs on the diamond substrate, the slope value was 6.32×10^{-3} which is 35, 168, and 1.02×10^4 times smaller than that on the Si, sapphire, and PI substrate, respectively. Similar trends were observed for the fall time of β-Ga_2O_3 NM SBDs on a diamond substrate compared with β-Ga_2O_3 NM SBDs on other substrates.

To further understand the heat dissipation effect on β-Ga_2O_3 NM SBDs, we performed a multiphysics simulation using the thermal module in COMSOL. The model structure was established using the same dimensional parameters and the empirical material parameters such as density, crystal structure, thermal resistance, and heat capacity from various references [8, 42-46]. In the simulation, the dissipated power was calculated as $P = V_{on} \times I_{on}$, where I_{on} is on state current and V_{on} is the corresponding bias. The actual biasing point was 3 mA at 4 V for all devices, and thus, an input power density of 12 mW was added to the electrode with a simulated structure. The initial temperature of the entire structure was set to 293.15 K as a boundary condition. Figure 5 and Figure S2 present the heat distribution of β-Ga_2O_3 NMs with 100 nm, 500 nm, and 1000 nm thicknesses under various substrates in the equilibrium state and the transit state at 1 μs. As shown in Figure 5, the local temperature at the electrode/β-Ga_2O_3 NM interface tends to rise higher when β-Ga_2O_3 NM SBDs are on a lower-k substrate. The interface temperature of β-Ga_2O_3 NM SBDs on the diamond, Si, sapphire, and PI substrate under

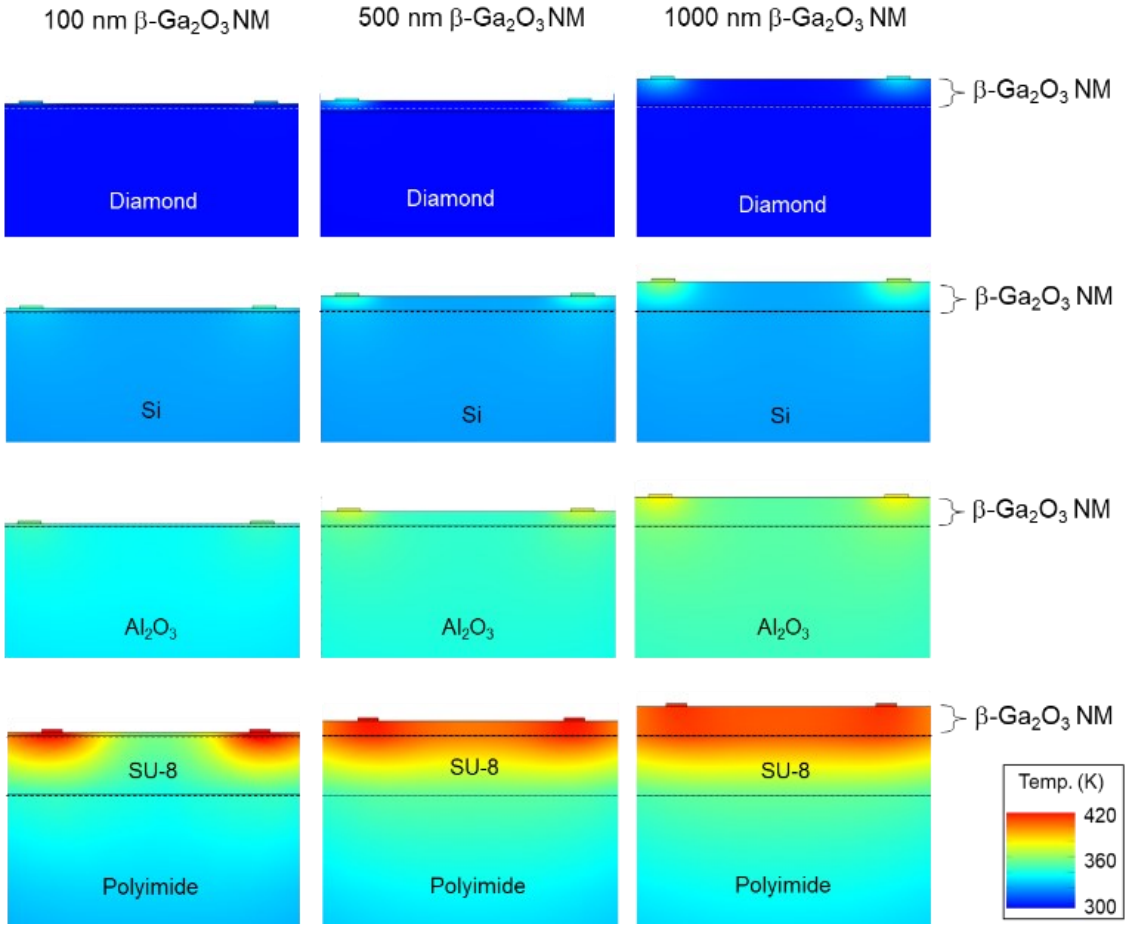

Figure 5. Simulated temperature profiles of β-Ga_2O_3 NMs on four different substrates and three different β-Ga_2O_3 NM thicknesses.

biasing conditions were calculated to be 298 K, 334 K, 365 K, and 420 K, respectively, which suggests that efficient heat dissipation can occur, or that the higher power can be handled when β-Ga_2O_3 devices are built on a high-k substrate. In addition, the heat distributions for various β-Ga_2O_3 NM thicknesses on different substrates were simulated.

Each row from left to right in Figure 5 shows the simulation result with 100 nm, 500 nm, and 1000 nm thick β-Ga_2O_3 NM on different substrates. In this simulation, we used the empirical thermal conductivity values of β-Ga_2O_3 NM by Yixiong et al. and Zheng et al. [8, 28], which shows a decreasing trend in thermal conductivity of β-Ga_2O_3 NM from 8.7 W/m·K for a 1000 nm thick β-Ga_2O_3 NM to 3.1 W/m·K for a 100 nm thick β-Ga_2O_3 NM. The thermal conductivity decreases smaller as the β-Ga_2O_3 NM thickness decreases, and a higher temperature in the β-Ga_2O_3 NM is expected as the thickness of β-Ga_2O_3 NMs decreases. However, the simulation result revealed that the electrode/β-Ga_2O_3 NM interface temperature decreases as the β-Ga_2O_3 NM thickness decreases. While the thermal conductivity of thinner β-Ga_2O_3 NMs is less than that of a thicker NM (i.e., 8.7 W/m·K for 1000 nm thick β-Ga_2O_3 NM and 3.1 W/m·K for 100 nm thick β-Ga_2O_3 NM), β-Ga_2O_3 NMs are prone to undergo heating as the β-Ga_2O_3 NM becomes thinner, and faster heat dissipation could occur when the β-Ga_2O_3 NMs are thinner and built on a high-k substrate. The simulation result suggests that devices with a thin β-Ga_2O_3 NM can dissipate heat faster through a high-k substrate which is important to prevent the device from overheating during a biasing condition. While this relationship affects better heat dissipation in β-Ga_2O_3 NMs, it should be noted that implanting a high-k substrate is more effective and primary way for the heat dissipation from the β-Ga_2O_3 NM than thinning down the β-Ga_2O_3 NM layer.

Table 1. Thermal conductivity values of substrates and β-Ga_2O_3 used in the simulation.

Substrate	TC
PI [44]	0.25 W/m·K
SU-8 [46]	0.2 W/m·K
Si [43]	144 W/m·K
Sapphire [42]	40 W/m·K
Diamond [45]	2200 W/m·K
β-Ga_2O_3 NM [8]	3.1 W/m·K (100 nm), 5.2 W/m·K (500 nm), 8.68 W/m·K (1000 nm)

Figure 3 and the simulated temperature profiles shown in Figure 5 offer a useful design aspect of β-Ga_2O_3 NM devices. For example, as shown in Figures 2 and 3, the diamond substrate offers the best heat dissipation due to the inherent high thermal conductivity. However, the largest single-crystal diamond substrate available on the market is less than 1 cm^2 and it is also expensive. Therefore, despite its' excellent thermal properties, choosing a diamond substrate as a heat dissipator is not a cost-effective option in commercial power applications. In this regard, Figure 3 with the support of Figure 5 provides an alternative solution for the thermal management of β-Ga_2O_3 NM devices. For example, Figure 4 (a summary graph of Figure 2 and 3) illustrates alternative substrates with different β-Ga_2O_3 NM thicknesses from the product of the substrate thermal conductivity and β-Ga_2O_3 NM thickness. Therefore, the Si substrate (k=144 W/m·K) or SiC substrate (k=~300 W/m·K) with a slightly thicker β-Ga_2O_3 NM can offer a similar heat dissipation capability as that of the diamond substrate with a much larger substrate size.

On the other hands, the opposite trend was observed for β-Ga_2O_3 NM SBDs on the PI substrate, which represents a low-k substrate. In other words, the temperature at the electrode/β-Ga_2O_3 NM interface becomes heated several tens of degrees higher to 405 K, 413 K, and 420 K as the β-Ga_2O_3 NM thickness is reduced from 1000 nm to 500 nm and 100 nm, respectively. This opposite trend can be explained by the thermal conductivity of the β-Ga_2O_3 NM and PI substrate. As shown in Table 1, the thermal conductivity of β-Ga_2O_3 NMs (5 W/m·K on average) is much larger than the thermal conductivity of PI and SU-8 (0.25 and 0.2 W/m·K, respectively). Thus, heat dissipation occurs along with the β-Ga_2O_3 NM rather than through the PI substrate. Therefore, as the simulation result indicates, the integration of β-Ga_2O_3 NM with a low-k substrate degrades the contact resistance and affects the sheet resistance and overall bulk properties.

4. Conclusions

In conclusion, a transient delay in the rising and falling time of β-Ga_2O_3 NM SBDs that were formed on four different substrates were measured using a sub-micron second resolution time-resolved electrical measurement system under different temperature conditions. The devices exhibited noticeably less-delayed turn on/off transient time when β-Ga_2O_3 NM SBDs were transfer-printed on a high-*k* substrate. Furthermore, a relationship between the β-Ga_2O_3 NM thickness and its time-resolved electrical properties was systematically investigated, and thinner β-Ga_2O_3 NM showed better heat dissipation, although the thermal conductivity of thinner β-Ga_2O_3 NMs was smaller than that of thicker NMs. Overall, our results reveal the impact of various substrates with different thermal properties and different β-Ga_2O_3 NM thicknesses on the performance of β-Ga_2O_3 NM-based

devices. Thus, these results can guide future efforts to optimize the performance of β-Ga_2O_3 devices by maximizing heat dissipation from the β-Ga_2O_3 layer. Successful implementation of the high-*k* substrates on β-Ga_2O_3 devices will have a transformative impact on next-generation communications, power electronics, and optoelectronics. Additionally, the physical dimension (i.e., a thickness) of the β-Ga_2O_3 layer is a secondary factor that decides the effective heat dissipation. Combined, our results will enable the realization of a higher operation frequency in β-Ga_2O_3 RF devices as well as compact and efficient β-Ga_2O_3 power conversion systems.

Data availability statement

The data that support the findings of this study are available upon reasonable request from the authors.

Acknowledgements

This work was supported by the National Science Foundation (Grant number: ECCS-1809077).

References

[1] Sharma S, Zeng K, Saha S and Singisetti U 2020 Field-Plated Lateral Ga_2O_3 MOSFETs With Polymer Passivation and 8.03 kV Breakdown Voltage *IEEE Electron Device Letters* **41** 836-9.

[2] Hasan M N, Swinnich E and Seo J-H *Wide Bandgap Semiconductor Electronics and Devices,* pp 63-78.

[3] Pearton S J, Yang J, Cary P H, Ren F, Kim J, Tadjer M J and Mastro M A 2018 A review of Ga2O3 materials, processing, and devices *Applied Physics Reviews* **5** 011301.

[4] Higashiwaki M, Sasaki K, Kuramata A, Masui T and Yamakoshi S 2012 Gallium oxide (Ga2O3) metal-semiconductor field-effect transistors on single-crystal β-Ga2O3 (010) substrates *Applied Physics Letters* **100** 013504.

[5] Zeng K, Vaidya A and Singisetti U 2019 A field-plated Ga2O3 MOSFET with near 2-kV breakdown voltage and 520 mΩ· cm2 on-resistance *Applied Physics Express* **12** 081003.

[6] Green A J, Chabak K D, Baldini M, Moser N, Gilbert R, Fitch R C, Wagner G, Galazka Z, Mccandless J, Crespo A, Leedy K and Jessen G H 2017 β -Ga2O3 MOSFETs for Radio Frequency Operation *IEEE Electron Device Letters* **38** 790-3.

[7] Oh S, Kim C-K and Kim J 2018 High Responsivity β-Ga2O3 Metal–Semiconductor–Metal Solar-Blind Photodetectors with Ultraviolet Transparent Graphene Electrodes *ACS Photonics* **5** 1123-8.

[8] Zheng Y, Swinnich E and Seo J-H 2020 Investigation of Thermal Properties of β-Ga2O3 Nanomembranes on Diamond Heterostructure Using Raman Thermometry *ECS Journal of Solid State Science and Technology* **9** 055007.

[9] Guo Z, Verma A, Wu X, Sun F, Hickman A, Masui T, Kuramata A, Higashiwaki M, Jena D and Luo T 2015 Anisotropic thermal conductivity in single crystal β-gallium oxide *Applied Physics Letters* **106** 111909.

[10] Burgemeister E A, Muench W v and Pettenpaul E 1979 Thermal conductivity and electrical properties of 6H silicon carbide *Journal of Applied Physics* **50** 5790-4.

[11] Jackson T B, Virkar A V, More K L, Dinwiddie Jr. R B and Cutler R A 1997 High-Thermal-Conductivity Aluminum Nitride Ceramics: The Effect of Thermodynamic, Kinetic, and Microstructural Factors *Journal of the American Ceramic Society* **80** 1421-35.

[12] Zou J, Kotchetkov D, Balandin A A, Florescu D I and Pollak F H 2002 Thermal conductivity of GaN films: Effects of impurities and dislocations *Journal of Applied Physics* **92** 2534-9

[13] Pearton S J, Ren F, Tadjer M and Kim J 2018 Perspective: Ga2O3 for ultra-high power rectifiers and MOSFETS *Journal of Applied Physics* **124** 220901.

[14] Sharma R, Patrick E, Law M E, Yang J, Ren F and Pearton S J 2019 Thermal Simulations of High Current β-Ga2O3 Schottky Rectifiers *ECS Journal of Solid State Science and Technology* **8** Q3195-Q201.

[15] Zhou H, Maize K, Qiu G, Shakouri A and Ye P D 2017 β-Ga2O3 on insulator field-effect transistors with drain currents exceeding 1.5 A/mm and their self-heating effect *Applied Physics Letters* **111** 092102.

[16] Liu S E, Wang J S, Lu Y R, Huang D S, Huang C F, Hsieh W H, Lee J H, Tsai Y S, Shih J R, Lee Y H and Wu K 2014 Self-heating effect in FinFETs and its impact on devices reliability characterization. In: *2014 IEEE International Reliability Physics Symposium,* pp 4A..1-4A.

[17] Semenov O, Vassighi A and Sachdev M 2006 Impact of self-heating effect on long-term reliability and performance degradation in CMOS circuits *IEEE Transactions on Device and Materials Reliability* **6** 17-27

[18] Benbakhti B, Soltani A, Kalna K, Rousseau M and Jaeger J D 2009 Effects of Self-Heating on Performance Degradation in AlGaN/GaN-Based Devices *IEEE Transactions on Electron Devices* **56** 2178-85.

[19] Agaiby R, Yang Y, Olsen S H, O'Neill A G, Eneman G, Verheyen P, Loo R and Claeys C 2007 Quantifying self-heating effects with scaling in globally strained Si MOSFETs *Solid-State Electronics* **51** 1473-8.

[20] O'Neill A, Agaiby R, Olsen S, Yang Y, Hellstrom P E, Ostling M, Oehme M, Lyutovich K, Kasper E, Eneman G, Verheyen P, Loo R, Claeys C, Fiegna C and Sangiorgi E 2008 Reduced self-heating by strained silicon substrate engineering *Applied Surface Science* **254** 6182-5.

[21] Li X, Park W, Wang Y, Chen Y P and Ruan X 2019 Reducing interfacial thermal resistance between metal and dielectric materials by a metal interlayer *Journal of Applied Physics* **125** 045302.

[22] Shi J, Yuan C, Huang H-L, Johnson J, Chae C, Wang S, Hanus R, Kim S, Cheng Z, Hwang J and Graham S 2021 Thermal Transport across Metal/β-Ga2O3 Interfaces *ACS Applied Materials & Interfaces* **13** 29083-91.

[23] Montes J, Yang C, Fu H, Yang T-H, Fu K, Chen H, Zhou J, Huang X and Zhao Y 2019 Demonstration of mechanically exfoliated β-Ga2O3/GaN p-n heterojunction *Applied Physics Letters* **114** 162103

[24] Lai J, Hasan M N, Swinnich E, Tang Z, Shin S-H, Kim M, Zhang P and Seo J-H 2020 Flexible crystalline β-Ga2O3 solar-blind photodetectors *Journal of Materials Chemistry C* **8** 14732-9.

[25] Swinnich E, Hasan M N, Zeng K, Dove Y, Singisetti U, Mazumder B and Seo J-H 2019 Flexible β-Ga2O3

Nanomembrane Schottky Barrier Diodes *Advanced Electronic Materials* **5** 1800714.

[26] Hasan M N, Lai J, Swinnich E, Zheng Y, Baboukani B S, Nalam P C and Seo J-H 2021 Flexible Electronics: Investigation of Nano-Gaps in Fractured β-Ga2O3 Nanomembranes Formed by Uniaxial Strain (Adv. Electron. Mater. 2/2021) *Advanced Electronic Materials* **7** 2170006.

[27] Kim M, Seo J-H, Singisetti U and Ma Z 2017 Recent advances in free-standing single crystalline wide band-gap semiconductors and their applications: GaN, SiC, ZnO, β-Ga2O3, and diamond *Journal of Materials Chemistry C* **5** 8338-54.

[28] Zheng Y and Seo J-H 2020 A simplified method of measuring thermal conductivity of β-Ga2O3 nanomembrane *Nano Express* **1** 030010.

[29] Cheng Z, Yates L, Shi J, Tadjer M J, Hobart K D and Graham S 2019 Thermal conductance across β-Ga2O3-diamond van der Waals heterogeneous interfaces *APL Materials* **7** 031118.

[30] Zheng Y, Feng Z, Bhuiyan A F M A U, Meng L, Dhole S, Jia Q, Zhao H and Seo J-H 2021 Large-size free-standing single-crystal β-Ga2O3 membranes fabricated by hydrogen implantation and lift-off *Journal of Materials Chemistry C* **9** 6180-6.

[31] Cheng Z, Mu F, You T, Xu W, Shi J, Liao M E, Wang Y, Huynh K, Suga T, Goorsky M S, Ou X and Graham S 2020 Thermal Transport across Ion-Cut Monocrystalline β-Ga2O3 Thin Films and Bonded β-Ga2O3–SiC Interfaces *ACS Applied Materials & Interfaces* **12** 44943-51.

[32] Zheng Y, Hasan M N and Seo J-H 2021 High-Performance Solar Blind UV Photodetectors Based on Single-Crystal Si/β-Ga2O3 p-n Heterojunction *Advanced Materials Technologies* **6** 2100254.

[33] Herring C and Nichols M H 1949 Thermionic Emission *Reviews of Modern Physics* **21** 185-270.

[34] Woo H and Jeon S 2017 Microsecond Pulse I–V Approach to Understanding Defects in High Mobility Bi-layer Oxide Semiconductor Transistor *Scientific Reports* **7** 8235.

[35] Meneghesso G, Meneghini M, Bisi D, Rossetto I, Cester A, Mishra U K and Zanoni E 2013 Trapping phenomena in AlGaN/GaN HEMTs: a study based on pulsed and transient measurements *Semiconductor Science and Technology* **28** 074021.

[36] Haque N, Dalai S, Chatterjee B and Chakravorti S 2017 Studies of the effect of temperature on the charge trapping and de-trapping processes of polymeric insulators through depolarization current measurements *IEEE Transactions on Dielectrics and Electrical Insulation* **24** 1896-904.

[37] Islam M M, Adhikari N, Hernandez A, Janover A, Novak S, Agarwal S, Codding C L, Snure M, Huang M and Selim F A 2020 Direct measurement of the density and energy level of compensating acceptors and their impact on the conductivity of n-type Ga2O3 films *Journal of Applied Physics* **127** 145701.

[38] Islam M M, Rana D, Hernandez A, Haseman M and Selim F A 2019 Study of trap levels in β-Ga2O3 by thermoluminescence spectroscopy *Journal of Applied Physics* **125** 055701.

[39] Roy R, Hill V G and Osborn E F 1952 Polymorphism of Ga2O3 and the System Ga2O3—H2O *Journal of the American Chemical Society* **74** 719-22.

[40] Khan F, Cartier E, Kothandaraman C, Scott J C, Woo J C S and Iyer S S 2016 The Impact of Self-Heating on Charge Trapping in High-k-Metal-Gate nFETs *IEEE Electron Device Letters* **37** 88-91.

[41] Vaidya A and Singisetti U 2021 Temperature-Dependent Current Dispersion Study in β-Ga_2O_3 FETs Using Submicrosecond Pulsed I–V Characteristics *IEEE Transactions on Electron Devices* **68** 3755-61.

[42] Zhou H, Maize K, Noh J, Shakouri A and Ye P D 2017 Thermodynamic Studies of β-Ga2O3 Nanomembrane Field-Effect Transistors on a Sapphire Substrate *ACS Omega* **2** 7723-9.

[43] Glassbrenner C J and Slack G A 1964 Thermal Conductivity of Silicon and Germanium from 3°K to the Melting Point *Physical Review* **134** A1058-A69.

[44] Wang T, Wang M, Fu L, Duan Z, Chen Y, Hou X, Wu Y, Li S, Guo L, Kang R, Jiang N and Yu J 2018 Enhanced Thermal Conductivity of Polyimide Composites with Boron Nitride Nanosheets *Scientific Reports* **8** 1557.

[45] Sukhadolau A V, Ivakin E V, Ralchenko V G, Khomich A V, Vlasov A V and Popovich A F 2005 Thermal conductivity of CVD diamond at elevated temperatures *Diamond and Related Materials* **14** 589-93.

[46] Oh S H, Lee K-C, Chun J, Kim M and Lee S S 2001 Micro heat flux sensor using copper electroplating in SU-8 microstructures *Journal of Micromechanics and Microengineering* **11** 221-5.